*Journal of Imaging Science and Technology®* 51(4): 293–298, 2007.


# Gloss Granularity of Electrophotographic Prints

**J. S. Arney▲ and Ling Ye**
*Rochester Institute of Technology, Rochester, New York 14623*
*E-mail: arney@cis.rit.edu*

**Eric Maggard and Brian Renstrom**
*Hewlett-Packard Co., Boise, Idaho 83714*

**Abstract.** *The random variation in gloss often observed in images produced in electrophotographic printers has been examined by an analytical technique that combines the capabilities of a microdensitometer with a goniophotometer. The technique is called microgoniophotometry and measures both the spatial and the angular distribution of the specular component of reflected light. The analysis provides information about the spatial variation of specularly reflected light at all angles through which the specular light is reflected, not just at the equal/opposite angle at which gloss is traditionally measured. The results of this analysis have lead to an optical model of the random spatial variation in gloss. The results indicate that dry toner is typically not completely fused and can be described as a surface composed of two distinct regions. These two regions differ in the extent of fusing that has occurred, as manifested by their differences in specular reflectance characteristics. The difference in reflectance is manifested primarily in their different angular distributions of specular light and also in their spatial frequency. © 2007 Society for Imaging Science and Technology.*
[DOI: 10.2352/J.ImagingSci.Technol.(2007)51:4(293)]

## INTRODUCTION

A bidirectional reflectance distribution function (BRDF) is a useful way to characterize the angular distribution of specular light reflected from materials.[1–8] Moreover, one would expect the BRDF to be a necessary part of a complete instrumental characterization of visual attributes of gloss.[9] In addition to the angular distribution of the specular light, the spatial distribution of the specular light may also play a role in visual gloss.[10,11] As illustrated in Figure 1, gloss in electrophotographic prints is not always spatially uniform. Indeed, spatial variations in gloss take many forms. Artifacts such as streaking and banding are often observed in high gloss prints, and differential gloss involves differences in gloss between bordering regions of different color. The current report focuses on gloss granularity, which is the random gloss variation across a printed surface. Gloss granularity is illustrated in Fig. 1 with samples A and B showing different degrees of gloss granularity.

Granularity analysis is an analytical technique that evolved during the 20th century to characterize silver halide photographic film.[12] The typical microdensitometer was an optical microscope with a fixed aperture and an electronic light detector. The film sample was scanned under the microscope and a trace of irradiance versus location was recorded. This technique is called microdensitometry. Currently, a microdensitometry scan may be performed more easily by a software routine applied to a digital image captured with a camera and appropriate microscope optics.[13,14] Several reports have been published on the application of microdensitometry techniques to the analysis of gloss granularity.[10,11,15] All of these techniques involve detection of light at the specular angle (equal/opposite angle) while scanning across the surface of the sample. The current work extends this analytical technique to a measurement of the entire BRDF (goniophotometry) scanned spatially across the surface of a printed sample (microdensitometry). This analytical technique is called microgoniophotometry.

## THE MICROGONIOPHOTOMETER

The microgoniophotometer has been described in detail in previous reports and is summarized in Figure 2.[1,2,16–18] The print sample is wrapped around a cylinder, and this presents all sample angles from −90° to +90° to the camera. The sample is illuminated with a linear light source placed at an angle of 20° from the camera. This places a bright specular line at the half angle, $\theta = 10°$ between the camera and the source. Two images captured with this system are illustrated in Figure 3.

As illustrated in Fig. 3, the specular component of the reflected light maintains its polarization and is observed only

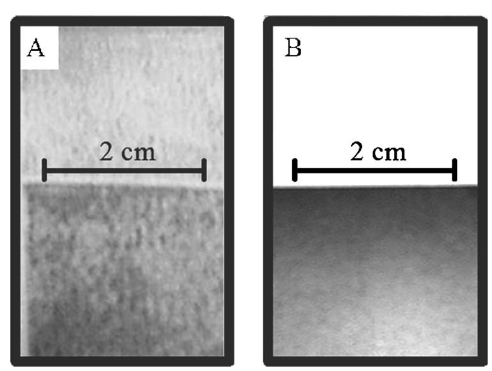


Figure 1. Examples of (A) rough and (B) smooth gloss granularity in electrophotographic prints produced by two different printers using different toners and fusing conditions.

▲IS&T Member

Received Jan. 3, 2007; accepted for publication Feb. 3, 2007.
1062-3701/2007/51(4)/293/6/$20.00.

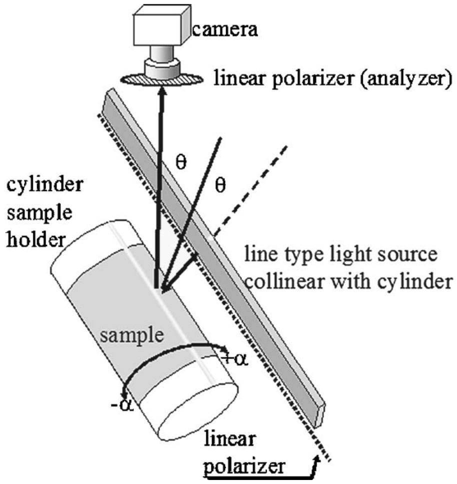


Figure 2. Schematic illustration of the microgoniophotometer. A linear polarizer is placed in front of the line light source, and another polarizer, called the analyzer, is in front of the camera.

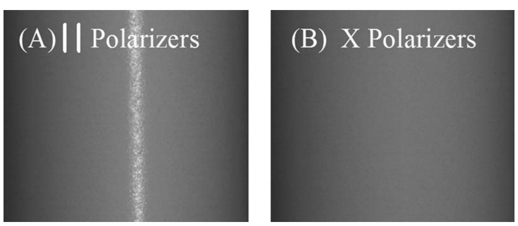


Figure 3. Images captured with the analyzer in front of the camera parallel to and perpendicular to the polarization direction of the light source polarizer.

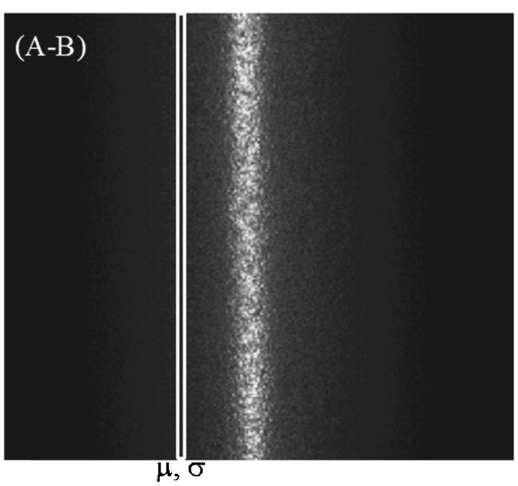


Figure 4. The difference image (A-B) shows only the specularly reflected light. The mean, $\mu$, and the standard deviation, $\sigma$, of the specular light is determined at each column in the image.

in the image with parallel polarizers. Both the crossed and the parallel polarizers capture the same amount of diffuse, randomly polarized light. The difference image, (A-B) in Figure 4, shows only the specular light.

The horizontal location of each column in the difference image (A-B) corresponds to a tilt angle, $\alpha$, on the print sample. A plot of the mean value versus tilt angle, $\mu$ vs $\alpha$, is a bidirectional reflectance distribution function, BRDF. A plot of the standard deviation versus tilt angle, $\sigma$ vs $\alpha$, is a bidirectional granularity distribution function, BGDF. (See Figure 5.) It is the granularity of the specular light at each angle on the BRDF.

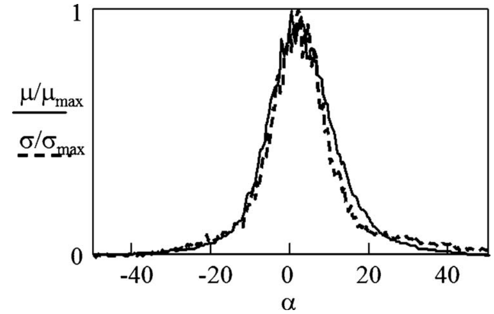


Figure 5. BRDF of $\mu$ vs $\alpha$ and BGDF of $\sigma$ vs $\alpha$ generated from Fig. 4. Curves are normalized to 1.00 at the peak value in order make a comparison.

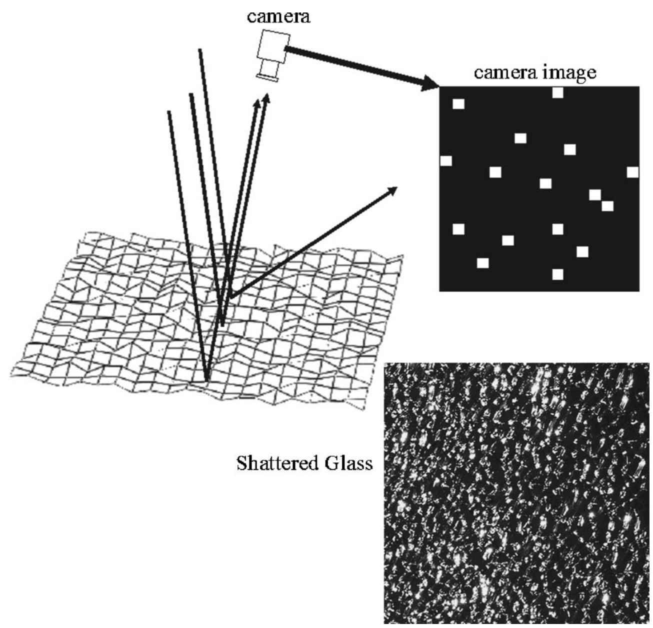


Figure 6. Microfacets of the surface are randomly oriented at different tilt angles. If the facet tilt results in an equal/opposite angle between the camera and the light source, then light enters the camera. Otherwise the specular light misses the camera. A piece of shattered automobile window glass is a macroscopic illustration of bilevel gloss granularity.

## A FACET MODEL OF SPECULAR GRANULARITY

Johansson, Béland, and MacGregor have introduced a model of specular reflection called the microfacet model,[10,11] and the microfacet model has been applied to the problem of synthetic scene generation in computer graphics.[19] The microfacet model assumes the surface that reflects the specular light can be described as a set of small facets, each at a randomly tilted angle, as illustrated schematically in Figure 6. The only facets that will deliver light to the camera are those facets tilted exactly to produces an equal/opposite

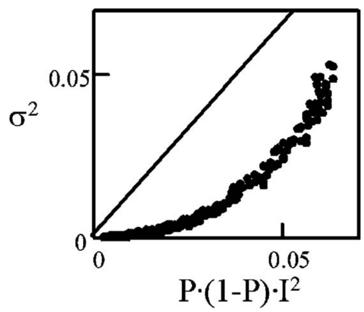


Figure 7. Example for a sample of solid black toner printed by a typical electrophotographic printer. The solid line is Eq. (3), and the points are from experimental measurements of $\mu$ and $\sigma^2$ over the range $-50° < \alpha < 50°$.

angle between the source and the camera. Otherwise the light misses the camera. The result would be expected to be the bilevel image of specular glints, as illustrated in Fig. 6.

The line light source used in the microgoniophotometer is assumed to be infinite in the direction colinear with the cylinder so that a facet tilt in the orthogonal direction, $\beta$, always directs light to the camera. Therefore, the BRDF measured with the microgoniophotometer should be a direct measure of the random distribution of facet tilt angles in the $\alpha$ direction. By normalizing the area under the BRDF, $\mu$ vs $\alpha$, to unity, the probability density function, $P(\alpha)$, for the random tilt angles, $\alpha$, can be formed as shown in Eqs. (1). The value of $P$ at each angle, $\alpha$, is a measure of the fraction of the surface that contains facets at exactly angle $\alpha$:

$$K = \int_{-90}^{90} \mu(\alpha) d\alpha \text{ and } P(\alpha) = \frac{\mu(\alpha)}{K}. \tag{1}$$

Each facet that is at the correct specular angle delivers light at irradiance $I$ to the camera. All other facets produce an irradiance of $I=0$. The result is irradiance $I$ at the facet location projected onto the camera sensor plane. This bilevel set of facets should produce an average value and a standard deviation given by Eqs. (2) and (3). Note from Eq. (1) that the area under the BRDF ($\mu$ vs $\alpha$) is an experimental measure of the irradiance, $I=K$,

$$\mu(\alpha) = P(\alpha) \cdot I, \quad \text{where } I = K, \tag{2}$$

$$\sigma^2(\alpha) = P(\alpha) \cdot [1 - P(\alpha)] \cdot I^2. \tag{3}$$

In order to test the facet model quantitatively, experimental measurements of $\sigma^2$ versus $\mu$ were carried out for twenty samples of solid black (single toner) produced by different printers with different toners and different fusing conditions on different substrates. Values of $P$ were calculated from $\mu$ with Eq. (1), and the data was plotted as $\sigma^2$ versus $P \cdot (1-P)$. Figure 7 is an example for a typical solid black toner printed by laser EP. The measured values of $\sigma^2$ were much lower than predicted, and the data do not show the linearity of Eq. (3). Thus the facet model illustrated in Fig. 6 does not provide a complete, quantitative rationale for the measured data.

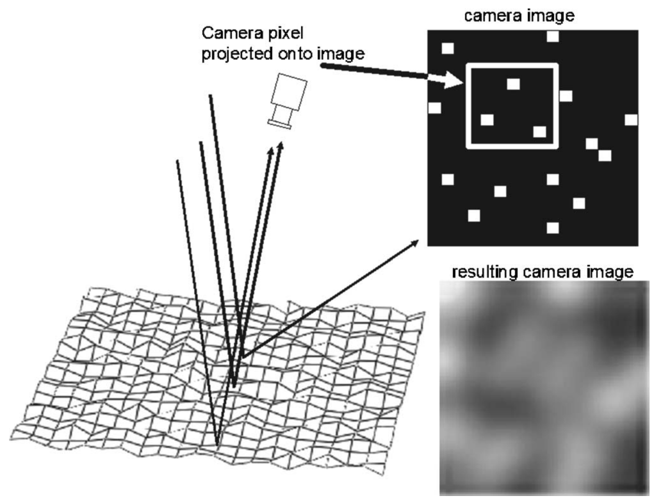


Figure 8. The blurring effect of the camera pixels projected onto the surface facets.

## AN EXPANDED FACET MODEL

It is not surprising that the experimentally measured values of $\sigma^2$ are lower than predicted. Equation (3) is based on the facets as if they were measured with infinite resolution. However, there is no reason to expect the surface facets to be large relative to the size of the camera pixels projected onto the surface. Indeed, if the camera pixels are larger than the facet size, the camera image will blur the image through a convolution with the effective aperture of the camera pixels. This is illustrated in Figure 8. The effect can be described quantitatively by modifying Eq. (3) with a blurring factor, $k$, as shown in Eq. (4):

$$\sigma^2(\alpha) = P(\alpha) \cdot [1 - P(\alpha)] \cdot I^2 \cdot k^2. \tag{4}$$

The nonlinearity observed in Fig. 7 requires additional modification of the facet model. Figure 9 suggests a modification based on the microstructure of the facets. Visual inspection of the printed samples in specular light indicates that the samples have a variety of different microstructures. Moreover, visual inspection of many samples suggests that the microstructures may be described as a population of two types of surfaces; one with well fused toner and the other with more poorly fused toner. This model is illustrated schematically in Figure 10.

These two regions would be expected to contribute to the overall measured BRDF and granularity of the sample. This is described in Eqs. (5)–(7), where $P_a$ and $P_b$ are the probability density functions for the distribution of surface tilt angles in the two regions illustrated in Fig. 10, $\sigma_a$ and $\sigma_b$ are the rms granularity characteristic of the two regions, and $F$ is the fraction of the surface that is region (a). Note that Eq. (7) reduces to Eq. (3) for $P_a = P_b$:

$$P(\alpha) = F \cdot P_a + (1 - F) \cdot P_b, \tag{5}$$

$$\sigma^2(\alpha) = F \cdot \sigma_a^2 \cdot I^2 + (1 - F) \cdot \sigma_b^2 \cdot I^2, \tag{6}$$

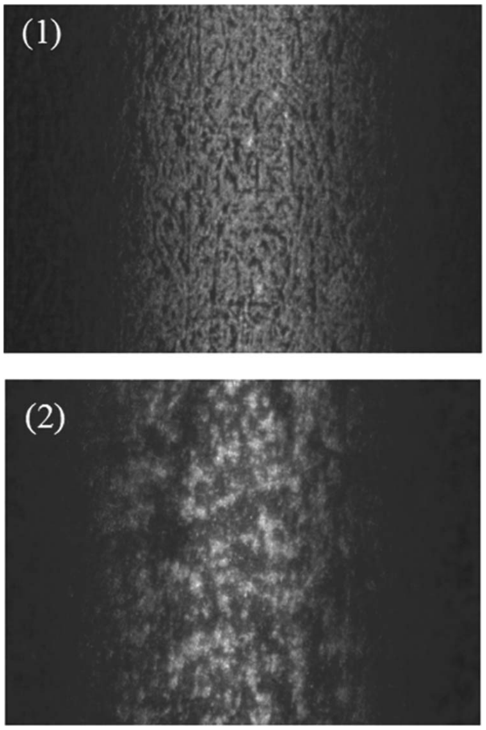


Figure 9. Closeup of the specular band for experimental samples 1 and 2.

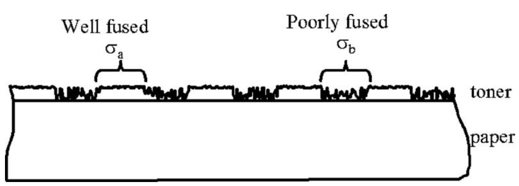


Figure 10. Schematic illustration of partial fusing of toner.

$$\sigma^2(\alpha) = F \cdot P_a \cdot (1 - P_a) \cdot I^2 + (1 - F) \cdot P_b \cdot (1 - P_b) \cdot I^2. \quad (7)$$

Equation (7) needs to be adjusted to account for the aperture effect of the camera pixels, as described above. However, one might expect the pixel aperture effect, the constant $k$ in Eq. (4), not to be the same for the two regions. Thus we write Eq. (7). Equations (5)–(8) represent an expanded facet model of specular reflections:

$$\sigma^2(\alpha) = F \cdot P_a \cdot (1 - P_a) \cdot I^2 \cdot k_a^2 + (1 - F) \cdot P_b \cdot (1 - P_b) \cdot I^2 \cdot k_b^2. \quad (8)$$

## APPLYING THE EXPANDED FACET MODEL

In order to model the BRDF and BGDF, the two individual PDF functions $P_a$ and $P_b$ are needed. These functions were assumed to be normal distributions described by Eqs. (9) and (10):

$$P_a(\alpha) = \frac{1}{s_a\sqrt{2\pi}} e^{-\alpha^2/2s_a^2}, \quad (9)$$

$$P_b(\alpha) = \frac{1}{s_b\sqrt{2\pi}} e^{-\alpha^2/2s_b^2}. \quad (10)$$

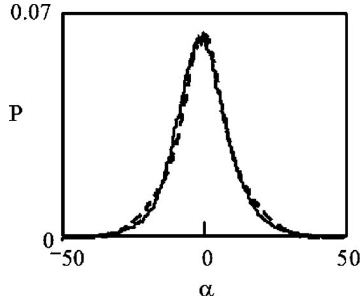


Figure 11. $P$ (normalized BRDF) versus angle $\alpha$ for a typical solid black printed by laser EP. The solid line is experimental data. The dotted line is the model of Eqs. (5), (9), and (10) with $s_a$=5.1°, $s_b$=12.7°, and $F$=0.3.

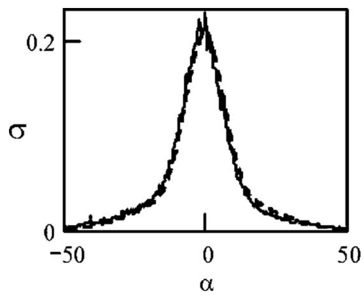


Figure 12. $\sigma$ (BRGF) versus angle $\alpha$ for a typical solid black printed by laser EP. The solid line is experimental data. The dotted line is the model of Eq. (8) with $k_a$=0.95 and $k_b$=0.20.

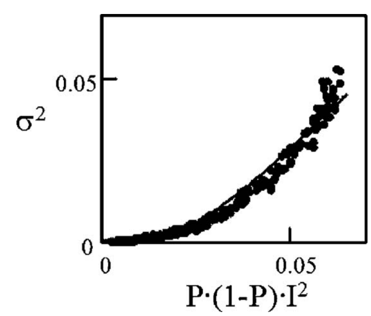


Figure 13. Example for a sample of solid black toner printed by a typical laser EP printer. The solid line is Eq. (3), and the points are from experimental measurements of $\mu$ and $\sigma^2$ over the range $-50° < \alpha < 50°$.

By combining Eqs. (5), (9), and (10), the BRDF can be modeled by adjusting the parameters, $s_a$, $s_b$, and $F$ to achieve the best fit with the experimental data. Figure 11 shows the result for one of the printed samples. The model parameters $s_a$, $s_b$, and $F$ were adjusted to achieve the minimum rms deviation from the experimental data.

Equation (8) has two additional parameters, $k_a$ and $k_b$, that must be adjusted to model the BGDF, $\sigma$ versus $\alpha$. Figure 12 shows the minimum rms deviation between the model and the data, and Figure 13 shows the corresponding plot of $\sigma$ versus $P$. The model provides a rationale for the significant deviation from linearity predicted by Eq. (3).

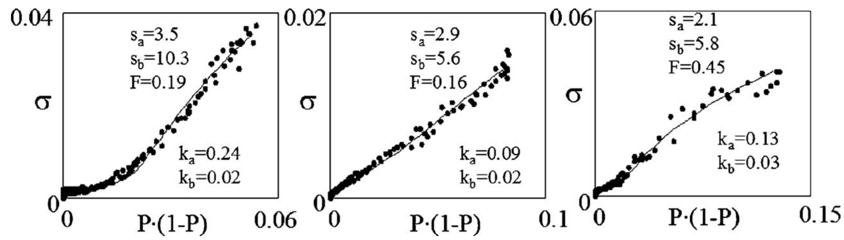


Figure 14. Examples of differences in behavior observed and modeled for other solid samples of black toner from different printers. Model parameters for $s_a$, $s_b$, $F$, $k_a$, and $k_b$ are also shown.

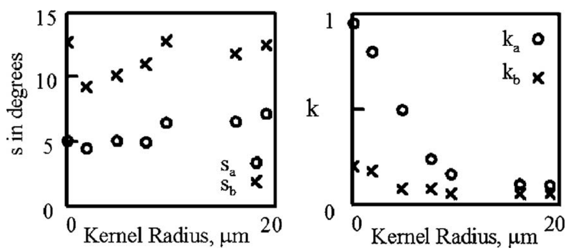


Figure 15. Values of $s_a$, $s_b$, $k_a$, and $k_b$ for a printed sample of black toner analyzed through low pass filters of radius $0 \leq R \leq 20$ $\mu$m.

## SPATIAL SIGNIFICANCE OF PARAMETERS $k_a$ AND $k_b$

Figure 14 illustrates the behavior of three additional samples of solid black toner printed by different electrophotographic printers. The differences in behavior are more easily observed by plotting $\sigma$ versus $P\cdot(1-P)$. The solid lines show the models that best fit the data, and the modeled values of $s_a$, $s_b$, $F$, $k_a$, and $k_b$ are also shown. From an analysis of 15 samples of black toner produced in different printers, this behavior appears to be representative of typical electrophotographic samples.

The physical meanings of parameters $\sigma_a$, $\sigma_b$, and $F$ are indicated in the diagram of Fig. 10. In all cases $s_a < s_b$, which suggests that the range of surface tilt angles in region (a) is less than the range of angles in region (b). This is reasonable if the toner in region (a) is more thoroughly fused than region (b). The fraction $F$ in every case is less than 0.5, which suggests that there is less of the smooth region (a) than of the more rough region (b).

The physical meaning of the parameters $k_a$ and $k_b$ is less obvious. In every case $k_a > k_b$. This suggests the effect of the pixel aperture convolution with the facet size has more of a blurring effect in the rough region (b) than in the smooth region (a). A possible rationale for this observation may be that the rough region (b) is also a higher frequency region. The low pass filtering effect of the pixel aperture would indeed be expected to have a have a larger effect on the higher frequency region (b) than the lower frequency region (a). Thus $k_a$ and $k_b$ provide spatial information about the gloss granularity in addition to the magnitude parameters $s_a$ and $s_b$.

As a check of the interpretation of $k_a$ and $k_b$ as indices of relative spatial frequency, the (A) image illustrated in Fig. 3 was low-pass filtered with a Gaussian kernel of radius $R$. Values of $R$ were selected over the range $R=0$ (no filtering) to $R=20$ $\mu$m. Each image was analyzed to extract experimental values of $\mu$ and $\sigma$ as described above, and from fitting the model to each data set, values of the model parameters were determined as described above. The results are shown in Figure 15. As one would expect, the smoothing kernel had only a small effect on the width parameters, $s_a$ and $s_b$. However, the values of $k_a$ and $k_b$ declined significantly, with $k_a$ decreasing much more than $k_b$.

## DISCUSSION

The behavior shown in Fig. 15 is consistent with the interpretation of $k_a$ and $k_b$ as noise attenuation factors related to the low pass filtering effect of the effective pixel aperture and the assumption that facets in the smooth region (a) are larger (lower frequency) than those in less well fused regions (b). The smaller facets in region (b) are low pass filtered to a larger extent than those in region (b) by the pixel aperture effect, so $k_b < k_a$. Further filtering by the added Gaussian filters lowers both $k_a$ and $k_b$, as expected, and they approach the same values for extreme low-pass filtering ($R=20$ $\mu$m).

As discussed in a previous report, the width of the BRDF is an inverse index of traditional gloss.[13] A narrow curve correlates with a high gloss reading. In the current work, it appears that fused toner can be interpreted in terms of two spatial regions that differ in the degree of fusing. The well fused region has a narrow BRDF, indicated by the value of $s_a$, and the poorly fused region has a broader BRDF indicated by $s_b$. The magnitude of the rms deviation of gloss, called gloss granularity, is indicated by the values of $k_a$ and $k_b$. As is typical of granularity indices, their magnitude is dependent on the effective spatial aperture of measurement. In this case that spatial aperture is the area of a camera pixel projected onto the surface. The range of behaviors of $k_a$ and $k_b$ observed in these experiments indicates that gloss granularity has a significant spatial frequency component that remains to be examined in future research.

## REFERENCES


1. J. S. Arney and Hung Tran, "An inexpensive micro-goniophotometry you can build", *Proc. IS&T's PICS Conference on Digital Image Capture, Reproduction, and Image Quality* (IS&T, Springfield, VA, 2002) pp. 179–182.
2. J. S. Arney, H. Hoon, and P. G. Anderson, "A micro-goniophotometer and the measurement of print gloss", J. Imaging Sci. Technol. **48**, 458 (2003).
3. J. M. Bennett and L. Mattsson, *Introduction to Surface Roughness and Scattering*, 2nd ed. (Optical Soc. of America, Washington, DC, 1999), Chap. 3.
4. J. C. Stover, *Optical Scattering, Measurement and Analysis* (McGraw Hill, NY, 1990).
5. I. Nimeroff, "Two-parameter gloss methods", J. Res. Natl. Bur. Stand.

**58**(3), 127 (1957).
[6] Standard Practice for Angle Resolved Optical Scatter Measurements on Specular or Diffuse Surfaces, Standard Procedure No. E 1392-96, American Society for Testing and Materials, 1996.
[7] I. Nimeroff, "Analysis of goniophotometric reflection curves", J. Res. Natl. Bur. Stand. **48**(6), 441 (1952).
[8] H. Rothe and D. Huester, "Application of circular and spherical statistics for the interpretation of BRDF measurements", Proc. SPIE **3141**(02), 13 (1997).
[9] M. Colbert, S. Pattanaik, and J. Krivanek, "BRDF-shop: creating physically correct bidirectional reflectance distribution functions", IEEE Comput. Graphics Appl. **26**(1), 30 (2006).
[10] P.-Å. Johansson, "Optical homogeneity of prints", doctoral thesis, KTH, Royal Institute of Technology, Stockholm, Sweden, 1999.
[11] M.-C. Béland, "Gloss variation of printed paper: relationship between topography and light scattering", doctoral thesis, KTH, Royal Institute of Technology, Stockholm, Sweden, 2001.
[12] R. E. Swing, *An Introduction to Microdensitometry* (SPIE Optical Engineering Press, Bellingham, WA, 1998).
[13] J. S. Arney, P. G. Engeldrum, and H. Zeng, "An Expanded Murray-Davies model of tone reproduction in halftone imaging", J. Imaging Sci. Technol. **39**, 502 (1995).
[14] J. S. Arney, C. Scigaj, and P. Mehta, "Linear color addition in halftones", J. Imaging Sci. Technol. **45**, 426 (2001).
[15] Y. Kipman, P. Mehta, K. Johnson, and D. Wolin, "A new method of measuring gloss mottle and micro-gloss using a line-scan CCD camera based imaging system", *Proc. IS&T's NIP17* (IS&T, Springfield, VA, 2001) p. 714.
[16] J. S. Arney, L. Ye, and S. Banach, "Interpretation of gloss meter measurements", J. Imaging Sci. Technol. **50**(6), 567 (2006).
[17] J. S. Arney, P. G. Anderson, G. Franz, and W. Pfeister, "Color properties of specular reflections", J. Imaging Sci. Technol. **50**(3), 228 (2006).
[18] J. S. Arney, L. Ye, J. Wible, and T. Oswald, "Analysis of paper gloss", J. Pulp Pap. Sci. **32**(1), 19 (2006).
[19] M. Ashikhmin, S. Premoze, and P. Shirley, "A microfaceted-based BRDF generator," *Proc. SIGGRAPH* (ACM Press, NY, 2000) pp. 65–74.